Chapter 5

Transport properties

In this chapter results of transport measurements are also been presented in the range of low to room temperature using the four probe method. Suitable modelswere fitted to explain the conduction mechanism. The same is correlated with the a.c. conductivities of the samples measured through dielectric measurements.

5.1 Electrical transport properties of pure and doped $CuFeO_2$ samples

The observed local distortions and changes in dipole moments due to thedoping of the CuFeO2samples were observed through Raman and Mossbauer studies in these samples. This can also have potential effects on the transport properties.

5.1.1 DC resistivity studies of pure and doped $CuFeO_2$ samples

Figure 5.1 represents the measured electrical resistivity as a function of temperature for pure and doped $CuFeO_2$ samples within the temperature range of 240 K to 300 K. The measurements were performed using the conventional four-probe method. It can be clearly seen from the plot that the resistivity of the samples decreases with anincrease in temperature, which suggests the semiconductor-like behavior of the samples. Also, there is a decrease in the resistivity due to doping of the pure $CuFeO_2$ samples. The values of resistivity of the samples at room temperature are given in table 5.1. Such value of resistivity of the n-type pure $CuFeO_2$ polycrystalline sample has been reported elsewhere [1].

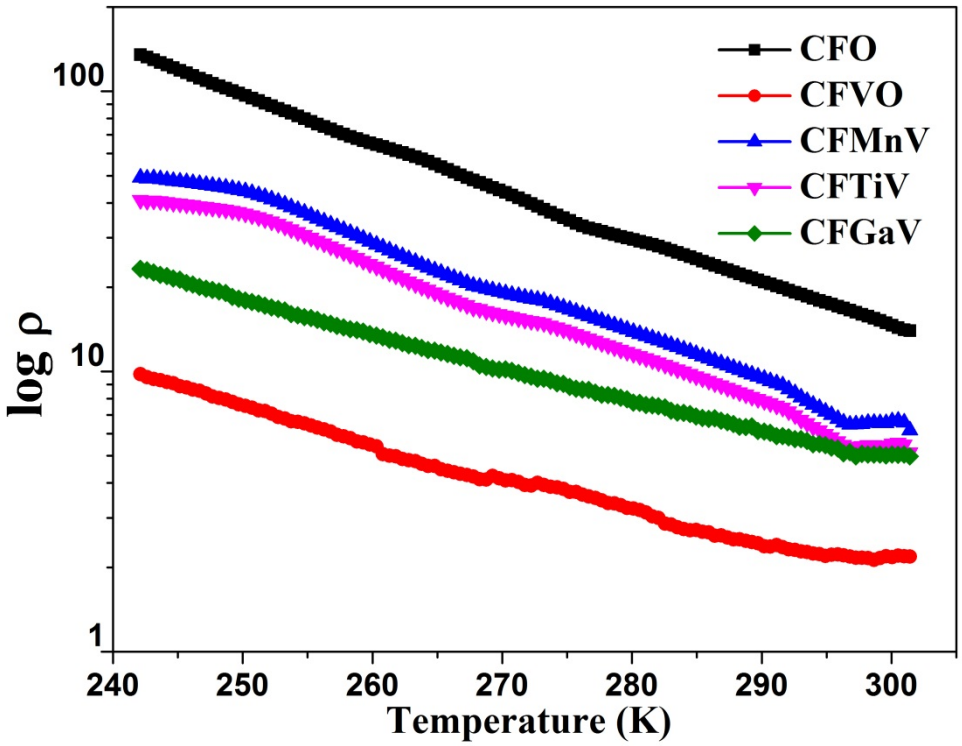

Figure 5.1: Temperature dependent resistivity of pure and doped $CuFeO_2$ samples

In the samples, the small polaron hopping (SPH) model can be applied to understand the conduction mechanism in the measured temperature range. It is pertinent for the conduction caused by the small polaron hopping using the thermal energy to the nearest neighbors [2].

The above mentioned model can be represented by the following equation:

$$\rho = \rho_0 T exp\left(\frac{E_A}{K_B T}\right) \qquad (5.1).$$

Where ρ_0 is the pre-exponential factor, which is independent of temperature, E_A is the activation energy, and k_B is the Boltzman constant [2–4]. The plot of $\ln(\rho/T)$ vs 1/T is a straight line. Theoretical fitting of the experimental data using the equation (5.1) (figure 5.2) shows that the SPH model is invalid for the entire range of the temperature, specifically at the lower temperatures, for the pristine, Mn and Ti-doped samples. The activation energy of the samples has been estimated through the SPH model. The values of the activation energies of the doped samples are given in table 5.1. The obtained values of the activation energies do not follow the trends of the respective decrease in resistivity.

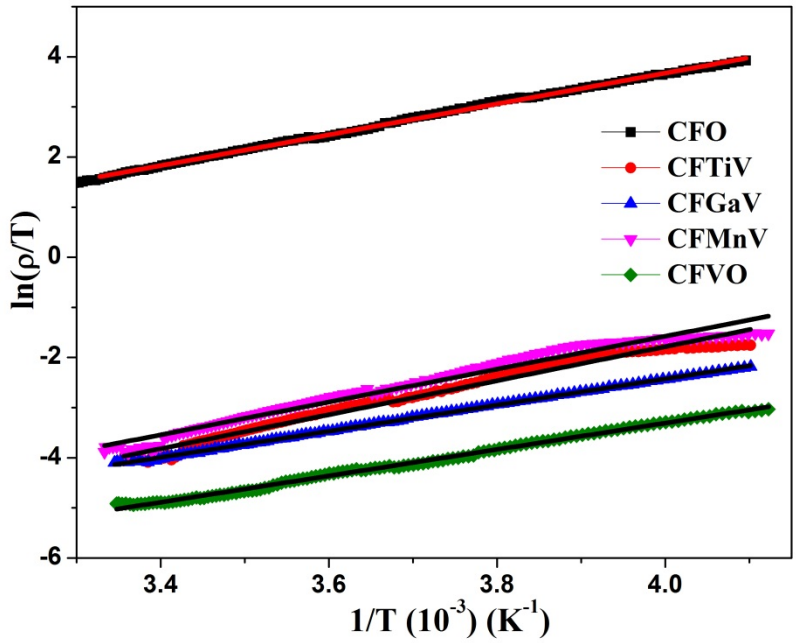

Figure 5.2: Graph of $\ln(\rho/T)$ vs 1/T gor the resistivity data fitting of SPH model

A negligible change in the values of the bandgap was observed, which suggests that the overall electronic band structure is unaffected along with insignificant change in the crystal structure (XRD data) due to doping. Although noteworthy changes in the conductivity provide aclear sign of changes in charge carrier concentration along with its mobility. Also, it is to be noted here that, though the level of doping of different elements is thesame, still there is variation in the percentage conductivity. Such a behavior is correlated with the Jahn-Teller distortions earlier observed through the Raman spectra and crystallite size variation. Furthermore, it may be taken into consideration that in the same temperature ranges minor changes in the lattice parameters are observed, which clearly signifies the role of doping-

induced changes in the charge concentration and its mobility rather than phonon mediated changes. In the present case Hall measurements provided inconsistent results due to the large resistivity and inbuilt inhomogeneity of these oxide systems when performed on bulk pallets. To overcome this problem a well-characterized thin film is required which can provide abetter solution. The above-observed changes in the mobility and charge carrier concentration linked to local distortions can all together result in changes in the multiferroic nature of the samples.

Table 5.1: Resistivity and activation energy of the studied samples

Sample	CFO	CFTiV	CFMnV	CFGaV	CFVO
Resistivity (Ω-m)	15.44	5.14	6.85	4.98	2.20
Activation energy (meV)	263.95	273.52	293.40	223.07	222.07

5.1.2 AC conductivity studies of pure and Ti-doped $CuFeO_2$ samples

The ac conductivity is the supportive measurement that provides more information regarding the nature of the conduction mechanism. The ac conductivity was calculated from the dielectric data, using the following equation [5,6]:

$$\sigma_{ac} = \varepsilon' \varepsilon_0 \omega \, tan\delta \qquad (5.2)$$

Where σ_{ac} = ac conductivity (ohm cm)$^{-1}$, ε' = Dielectric constant, ε_0= Permittivity of free space, $tan\delta$ = loss tangent, ω = angular frequency.

The graph of *log* σ_{ac} *vs 1000/T* is plotted within the temperature range of 10 K – 300 K and the selected frequencies (Fig. 5.3). It can be seen that the curve of ac conductivity seems to merge near the room temperature and is independent of the frequency (figure 5.4). The conductivity increases with an increase in temperature, which indicates the thermally activatedmechanism [6]. On the other hand at temperature <280 K, i.e., at lower temperature, the ac conductivity depends both on temperature and frequency. Further, it also been seen that the conductivity increases with anincrease in both temperature and frequency, thereby, suggesting the typical semiconducting nature of the samples [6,7] (figure 5.3). It is well reported that ac conductivity decreases with increase in frequency for large polaron hopping while it increases with anincrease in frequency for small polaron hopping [8–10]. From figure 5.3 it is clear that in the CFO and CFTiV samples the conductivity increases with an

increase in frequency which confirms that the conduction occurs essentially by the small polaron hopping, whose detailed study can be done using Jonscher's power law.

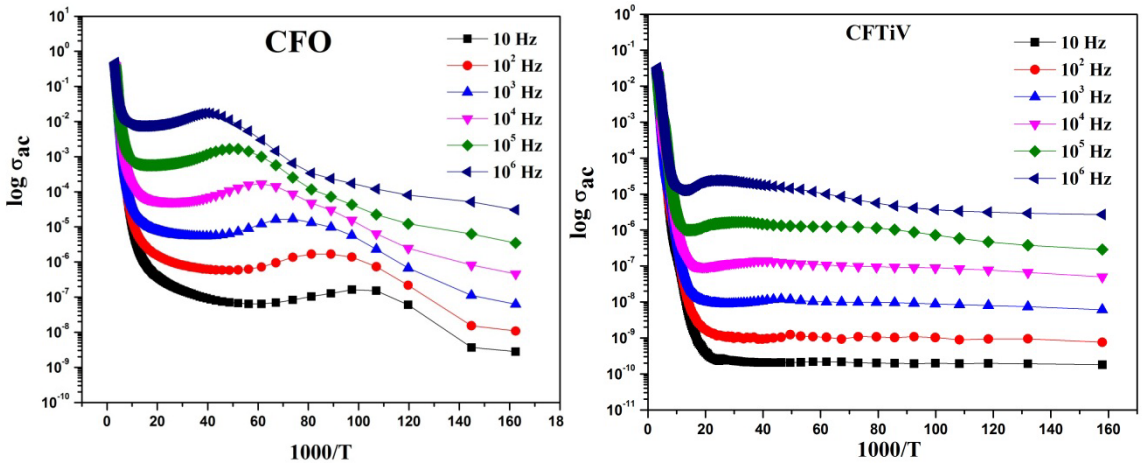

Figure 5.3: Variation of *log* σ_{ac} *vs 1000/T* for $CuFeO_2$ and $CuFe_{0.96}Ti_{0.03}V_{0.01}O_2$ sample

In the temperature region >280 K the plots of 10 Hz – 10^5 Hz seems to merge into a single curve. The activation energies have been calculated in the given region (figure 5.4) using thefollowing equation of Arrhenius law:

$$\sigma = \sigma_0 \exp\left(-\frac{E_a}{k_B T}\right) \qquad (5.3)$$

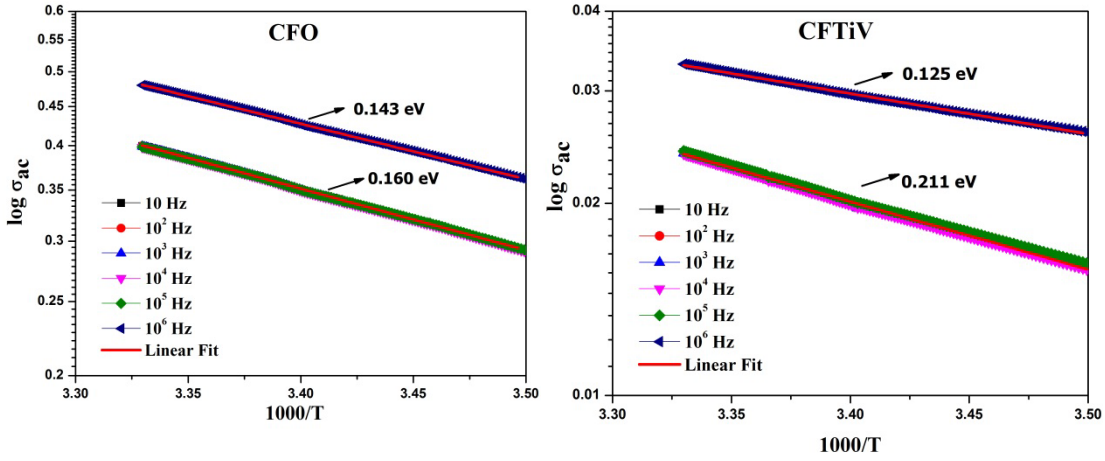

Figure 5.4: Variation of *log* σ_{ac} *vs 1000/T* for $CuFeO_2$ and $CuFe_{0.96}Ti_{0.03}V_{0.01}O_2$ samples near room temperature with linear fit for calculating activation energy

The slopes of the linear adjustment give the values of the activation energies. In general, it is observed that the ac activation energy in both the CFO and CFTiV samples havelower values at higher frequencies while higher values at lower frequencies. As at higher frequencies, the

hopping is restricted to nearest neighboring defects due to the smaller response time available to respond to external frequency, while hopping of charge carriers over long distances are responsible for the overall conductivities at low frequencies [6,11]. Higher activation energies are observed for CFTiV sample than CFO which again supports the finding of dc conductivity measurements and the degree of local distortion observed in the doped samples.

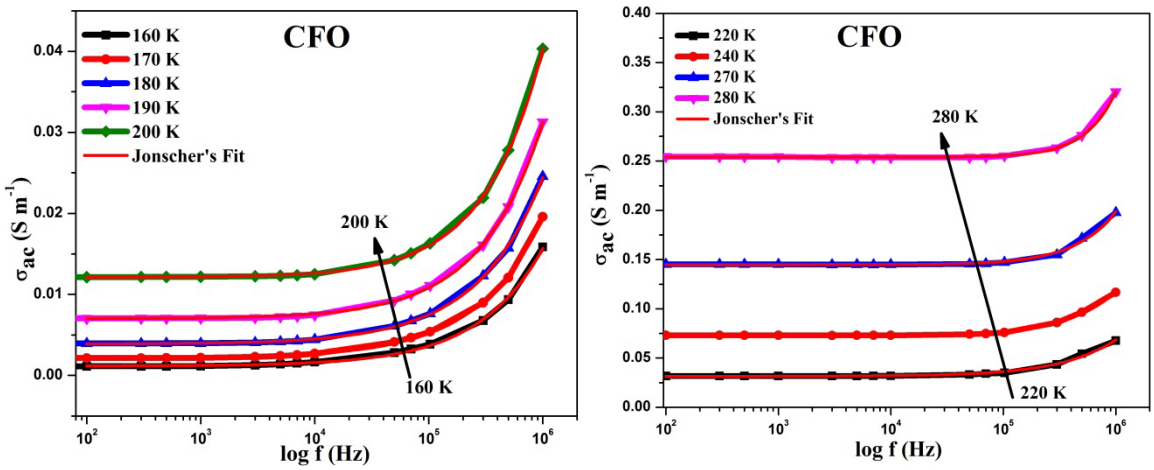

Figure 5.5: Plots of ac conductivity with respect to frequency and Johnscher's power law fit of $CuFeO_2$.

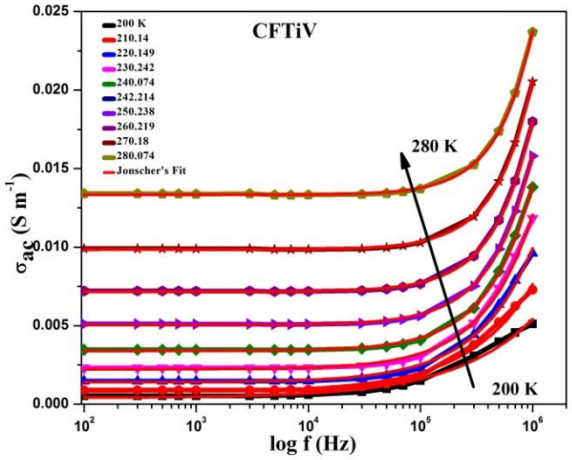

Figure 5.6: Plots of ac conductivity with respect to frequency and Johnscher's power law fit of $CuFeO_2$

The frequency dependence of electrical conductivity for CFO and CFTiV samples are presented in figures 5.5 and 5.6. It may be clearly observed that the conductivity increases with increase in frequency for both the samples confirming that the conduction is due to thesmall polaron hopping process [8,9]. One can also differentiate between two regions, a plateau region and a dispersion region. The plateau is at a low-frequency range corresponding to dc conductivity which increases with the rise temperature rise, thereby indicating a

thermally activated process. The dispersion region at high-frequency range corresponds to the ac conductivity. This nature can be attributed to the relaxation phenomena arising due to hopping of mobile charge carriers related to Jonscher's power law given by the following equation [12]:

$$\sigma_{ac} = \sigma_{dc} + A\omega^{n} \qquad (5.4)$$

Where σ_{ac} = ac conductivity; σ_{dc} = dc conductivity; A and n are pre-exponentialandexponential factors respectively.

Figures 5.5 and 5.6 show the jonscher's fitting of the curves of conductivity. The values of n ≤ 1 indicatethe presence of translational motion with sudden hopping and n > 1 indicates the presence of localized hopping [13]. For the present samples, the values of n have been varied within 0.85-1.60 for CFO and 0.61-1.37 for CFTiV.

The predominant conduction process in the samples can be studied by observing the variation of 'n' parameter with temperature. For CFO and CFTiV samples, the value of 'n' parameter increases with an increase in temperature indicates that the most appropriate model to describe the conductivity in the present samples is the small polaron tunneling model (NSPT) [14].

5.1.3 DC resistivity studies of pure and doped $CuCrO_2$ samples

The temperature-dependent electrical resistivity $\rho(T)$plots of the pristine and doped $CuCrO_2$ are shown in figures 5.7 and 5.8. Measurements were performed in the temperature range of 240 K to 300 K, and the plots clearly show the semiconducting nature of the samples. The resistivity of the samples decreases withincrease the temperature. Resistivity values at room temperature are shown in table 5.2. At room temperature,the resistivity value of the pristine $CuCrO_2$ sample is comparable to that reported elsewhere [15–17]. The hole as carriers mainly comes from the interstitial oxygen atoms in *p*-type delafossites [18–21].

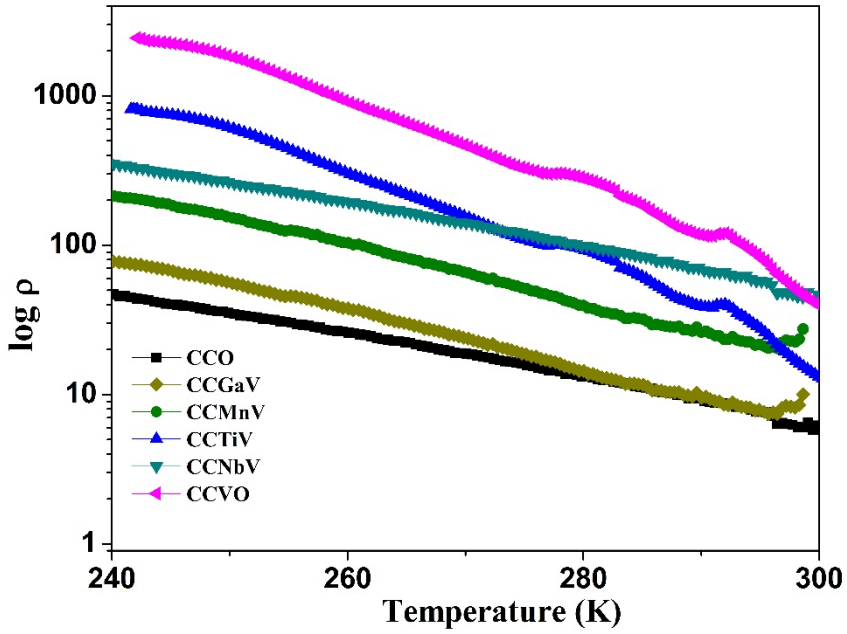

Figure 5.7: Temperature-dependent resistivity of $CuCrO_2$, $CuCr_{0.96}M_{0.03}V_{0.01}O_2$ (M = Ti, Mn, Ga, and Nb),and $CuCr_{0.96}V_{0.04}O_2$ samples.

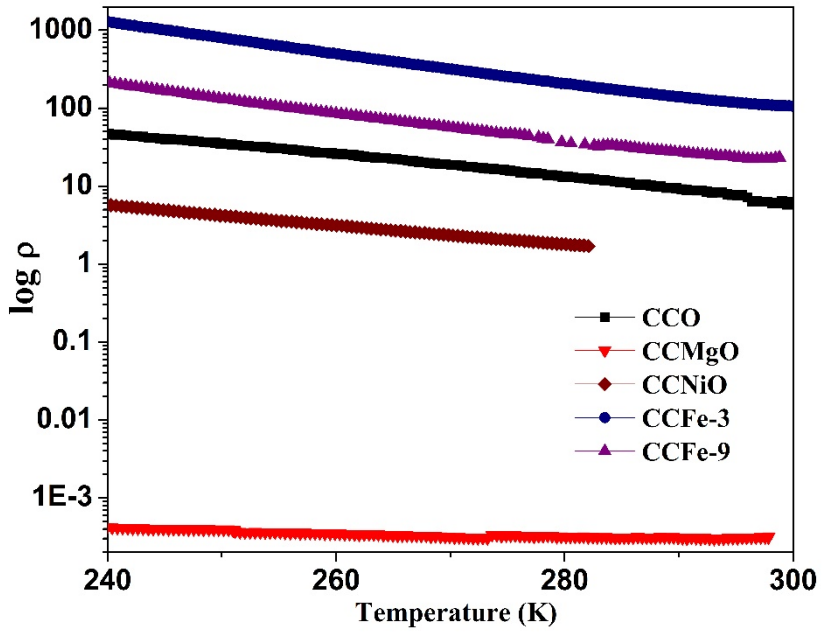

Figure 5.8: Temperature-dependent resistivity of $CuCrO_2$, $CuCr_{1-x}Fe_xO_2$ (x = 0.03 and 0.09), $CuCr_{0.97}Mg_{0.03}O_2$, and $CuCr_{0.97}Ni_{0.03}O_2$ samples.

It is worth mentioning that such a wide spectrum of doping in the $CuCrO_2$ compounds and resultant variations in $\rho(T)$ are,to the best of knowledge, reported for the first time. As pointed out earlier,the expected valency, based on ionic radii suitability, of dopants is greater than 3+, i.e., 4+ or 5+ or 3+/4+ mixture, will lead to doping of electrons. It can be seen in

figure 5.7 that when Cr^{3+} , based on ionic radii suitability, is substituted by either $Mn^{3+/4+}$(0.66/0.60A), Ti^{4+} (0.68A), V^{4+} (0.63A), or Nb^{5+} (0.63A), the resistivity increases considerably on lowering temperaturepresumably due to the compensation of electrons and holes as proposed earlier. The most drastic change is observed in 4% Vanadium doped samples, in which the resistivity value increases by a factor of about 50 at 240 K as compared to the pristine$CuCrO_2$ sample. This is presumably due to the reduction in the number of mobile holes. Further, the Ti^{4+}doping also showed enhanced resistivity at low temperatures, more than Nb^{5+}, probably because Titanium doping additionally exhibited a stronger lattice distortion whose evidence was revealed by Raman spectra and can be connected to the Jahn Taller effect [22]. On the other hand, doping of Ga^{3+} at Cr^{3+} site showed a relatively weak change in the temperature-dependent resistivity correlated with weakly observed distortions.

On the other handthe substitution of Cr^{3+} by a mixed of lower valence state ions, i.e., $Fe^{2+/3+}$ (0.64/0.74A), Mg^{2+} (0.66A), or Ni^{2+} (0.69A), the resistivity is drastically reduced. This is expected because the doping of additional holes induces more carriers in these semiconducting compounds. Earlier studies have also shown lowering of resistivity when Fe with 2+ valence is doped [16],whilean enhancement of resistivity when Fe^{3+} or Mn^{3+} is doped due to induced lattice distortions [22]. Here, it may be strongly commented that this method of selective mono/double doping can be a very useful tool to enhance the applicability of these delafossite semiconductors in various devices based on electrical conductivity and bandgap requirements. However,the bandgap modifications are complicated due to itsdependence on multiple factors such as metal-oxygen bond length, in-plane/out-of-plane hybridizations induced tilting of MO_6 hexagon, and effect of changes in nanosize crystallites. Based on the end applications of electron/hole doping, it is therefore,an effective way to control bandgap and carrier concentrations.

Table 5.2: Resistivity values measured at room temperature

Samples with electron doping						
Sample	CCO	CCGaV	CCMnV	CCTiV	CCNbV	CCVO
Resistivity (Ω-m)	6.0	8.2	20.3	21.6	45.9	53.3
Samples with hole doping						
Sample	CCO	CCMgO	CCNiO	CCFe-3	CCFe-9	
Resistivity (Ω-m)	6.0	1.0	2.0	110.3	21.4	

As explained earlier for CFO samples, two models viz. the variable hopping model (VRH) and the small polaron hopping model (SPH) are used to understand the conduction mechanism of the doped semiconductors. The VRH model is used when the thermal energy is not enough to excite the electrons to hop to their neighbors, and such electrons prefer to hop to a site with a smaller potential difference. The SPH model is applicable for the conduction taking place due to small polaron hopping, and carriers hop to the nearest neighbors assisted by thermal energy [2]. To understand the conduction mechanism in the presently investigated samples, we have applied the SPH model for the measured temperature range. This model can be represented by the following equation:

$$\rho = \rho_0 T \, exp\left(\frac{E_A}{k_B T}\right) \qquad (5.5)$$

Here ρ_0 is the pre-exponential factor which is independent of temperature, E_A is the activation energy andk_B is the Boltzmann constant [2,3,23]. According to the SPH model,a plot of ln(ρ/T) versus 1/T is expected to be a straight line. By fitting the experimental data for the presently investigated samples using equation 5.5 (figure 5.9 and 5.10), it can be seen that the SPH model is valid for the entire range of temperature investigated. Using the SPH model, we have estimated the activation energy,and it is given in table 5.3.The variation in the activation energy of the doped samples is in accordance with the observed data in figure 5.8.

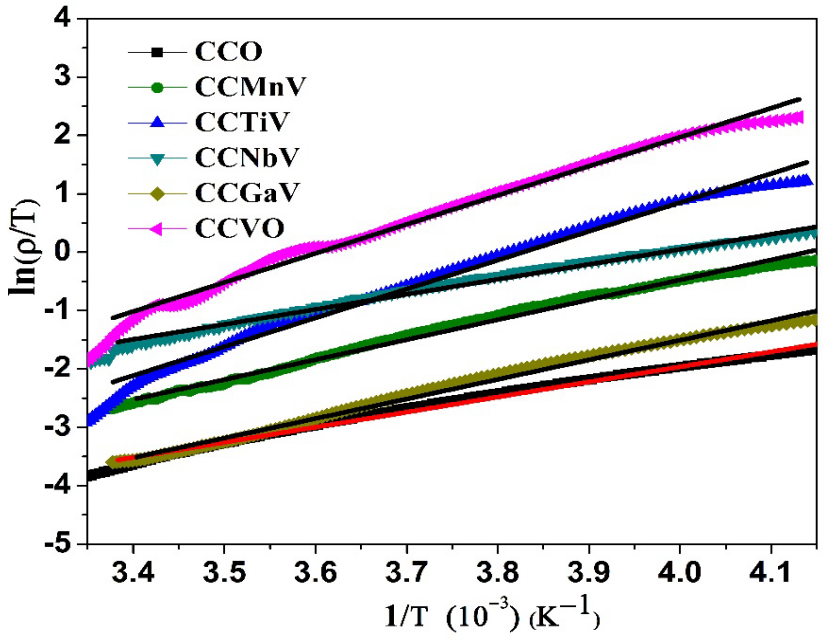

Figure 5.9: The plot of ln(ρ/T) versus 1/T for the resistivity data fitting by the SPH model of $CuCrO_2$ and $CuCr_{0.96}M_{0.03}V_{0.01}O_2$ (M = Ti, Mn, Ga, and Nb) samples.

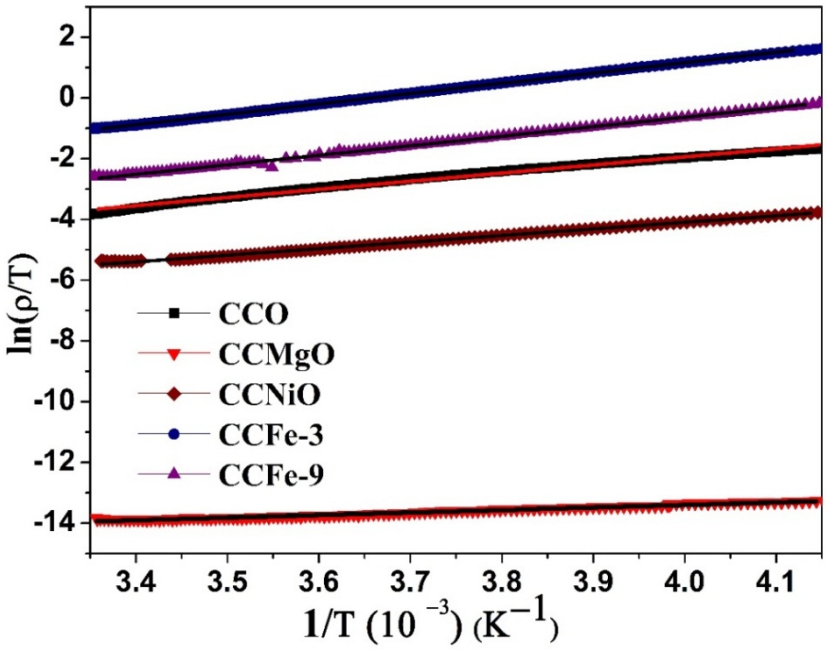

Figure 5.10: The plot of ln (ρ/T) versus 1/T for the resistivity data fitting of SPH model $CuCrO_2$, $CuCr_{1-x}Fe_xO_2$ (x = 0.03and 0.09), $CuCr_{0.97}Mg_{0.03}O_2$ and$CuCr_{0.97}Ni_{0.03}O_2$ samples.

Table 5.3: Activation energy for $CuCrO_2$, $CuCr_{0.96}M_{0.03}V_{0.01}O_2$ (M = Ti, Nb, Ga, and Mn), and $CuCr_{0.96}V_{0.04}O_2$ samples

Samples with electron doping						
Sample	CCO	CCGaV	CCMnV	CCTiV	CCNbV	CCVO
Activation energy (meV)	235.15	289.04	294.64	462.89	238.37	450.11
Samples with hole doping						
Sample	CCO	CCMgO	CCNiO	CCFe-3	CCFe-9	
Activation energy (meV)	235.15	71.10	186.92	287.19	259.66	

The contribution to the electrical conductivity of charge by lattice becomes negligibly small at very low temperatures leading to the confinement ofthe charges into various localized shells. These localized charges may induce magnetic dipole moment at low temperatures. Their mutual interactions can lead to interesting multiferroic properties in the undoped and doped $CuCrO_2$ compounds. Theelectron/hole doping induced optimization in the charge carrier concentration provides an ideal opportunity to extend a critical investigation of the

multiferroic properties, mainly the magnetic and dielectric properties, in these samples at low temperatures.

5.1.4 AC conductivity studies of pure and Ti-doped $CuCrO_2$ samples

The conduction mechanism can be further explained with the help of electrical conductivity measurements. The electrical conductivity can be calculated from the dielectric data using equation (5.2) as discussed earlier. The electrical conductivity of the present system with respect to temperature is presented in figures 5.11 and 5.12. It can be clearly seen that the ac conductivity seems to merge very near to room temperature and increases with an increase in temperature which suggests that near room temperature the conduction mechanism depends on temperature ratheron frequency that gradually decreases.

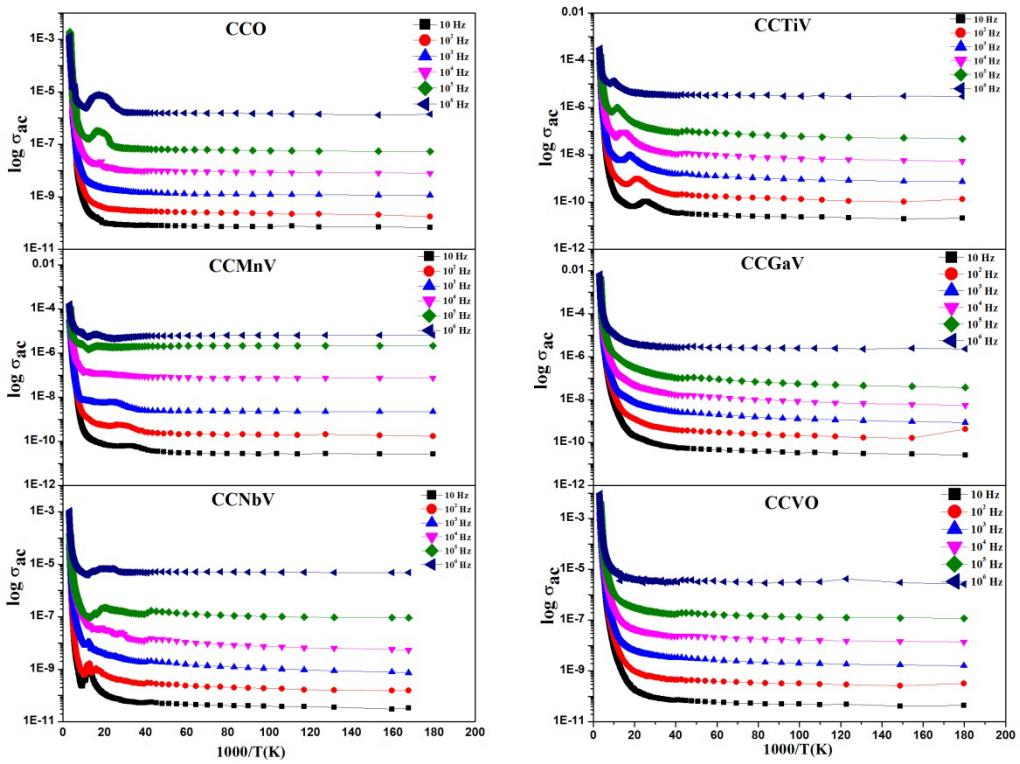

Figure 5.11: The plot of log σ_{ac} versus 1000/*T* for $CuCrO_2$ and $CuCr_{0.96}M_{0.03}V_{0.01}O_2$ (M = Ti, Mn, Ga, and Nb) and $CuCr_{0.96}V_{0.04}O_2$samples.

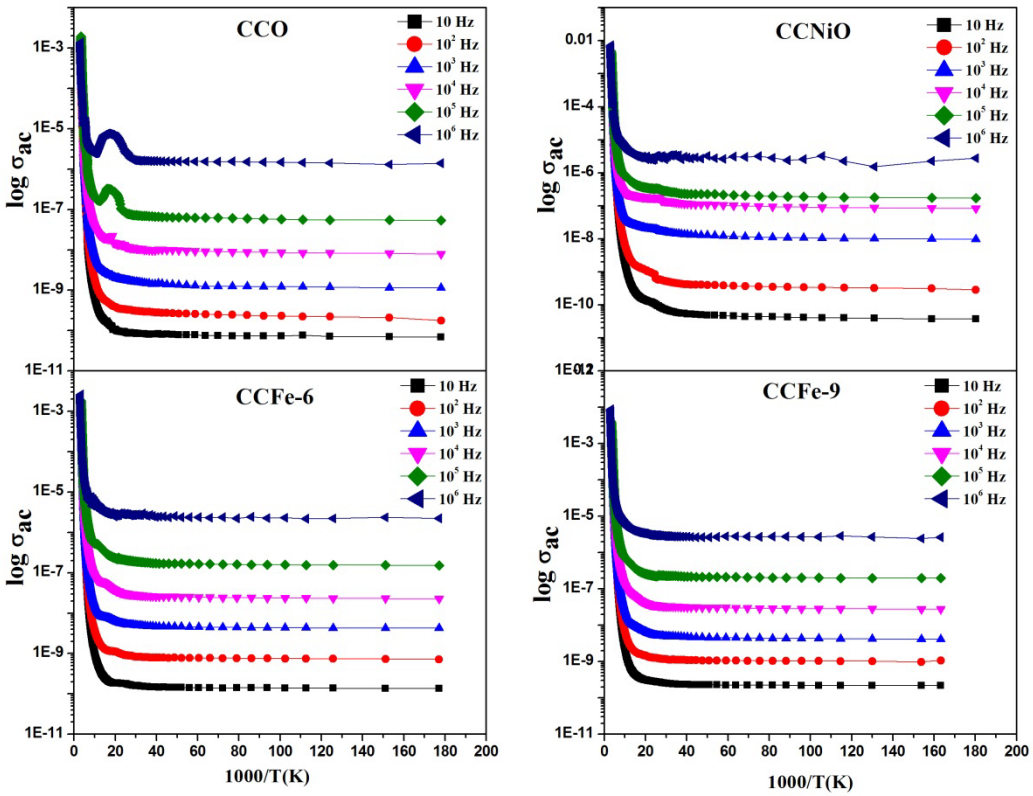

Figure 5.12: The plot of log σ_{ac} versus 1000/*T* for $CuCrO_2$ and $CuCr_{0.96}Ni_{0.04}O_2$and $CuCr_{1-x}FeO_2$(x = 0.06 and 0.09) samples.

For lower temperatures the conductivity depends on both temperature and frequency, i.e., the ac conductivity increases with the increase in frequency for a given temperature. Similarlythe ac conductivity increases with temperature for a given frequency. It clearly suggests that the conductivity in the system is due to small polaron hopping (SPH) [8,9].

The activation energy values can be deduced from the slopes of Arrhenius plots near the room temperature. Figures 5.11 and 5.12 show the linear fit of ac conductivity arrhenius plots for the doped and pure $CuCrO_2$ samples near room temperature. The deduced activation energies for the low and high frequencies are given in table 5.4. The values of activation energies werefound to be large at low as compared to higher frequencies. This can be attributed to the smaller response time available at high frequencies [6,11].

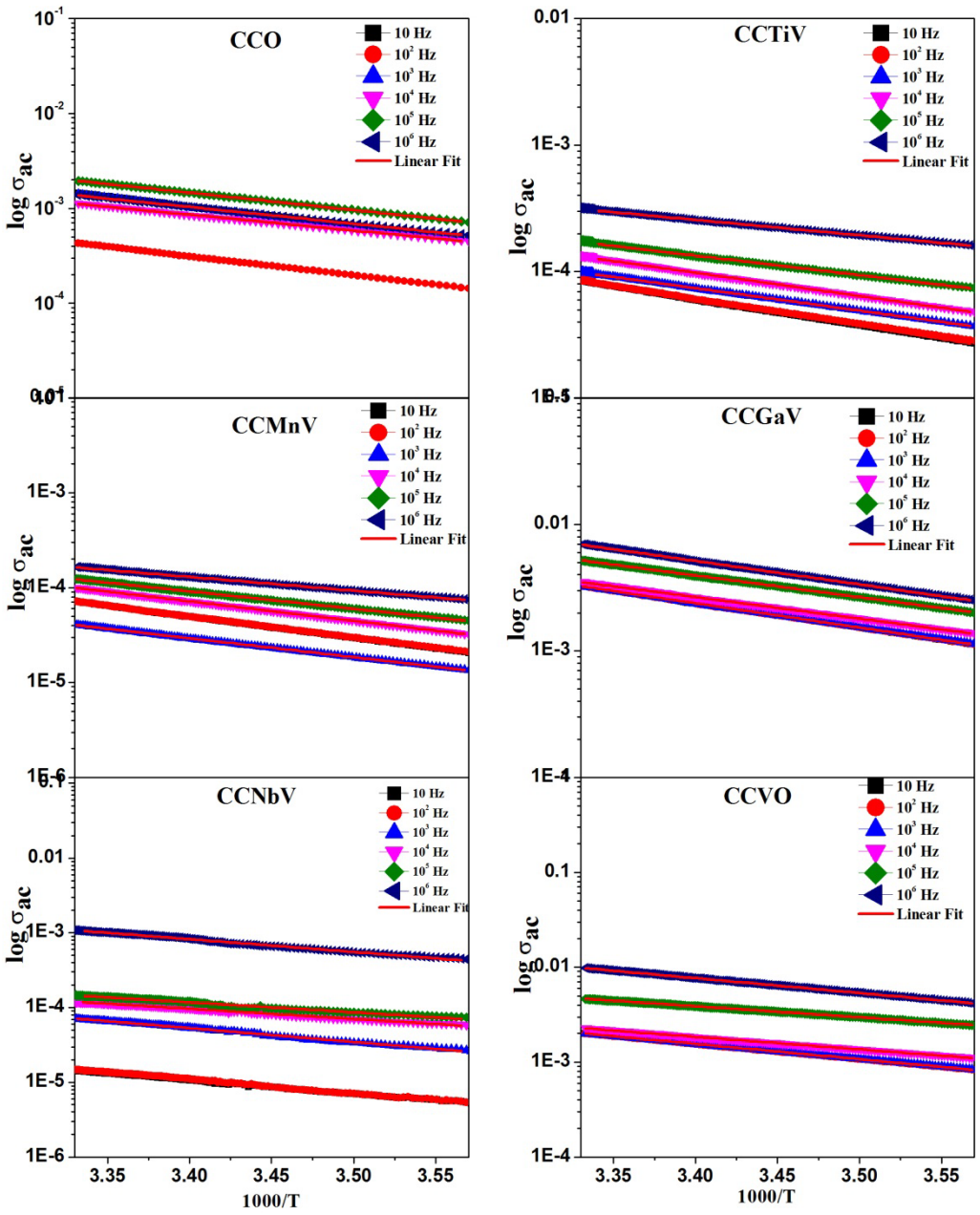

Figure 5. 13: Arrhenius liner fit for $CuCrO_2$ and $CuCr_{0.96}M_{0.03}V_{0.01}O_2$ (M = Ti, Mn, Ga, and Nb) and $CuCr_{0.96}V_{0.04}O_2$ samples near room temperature.

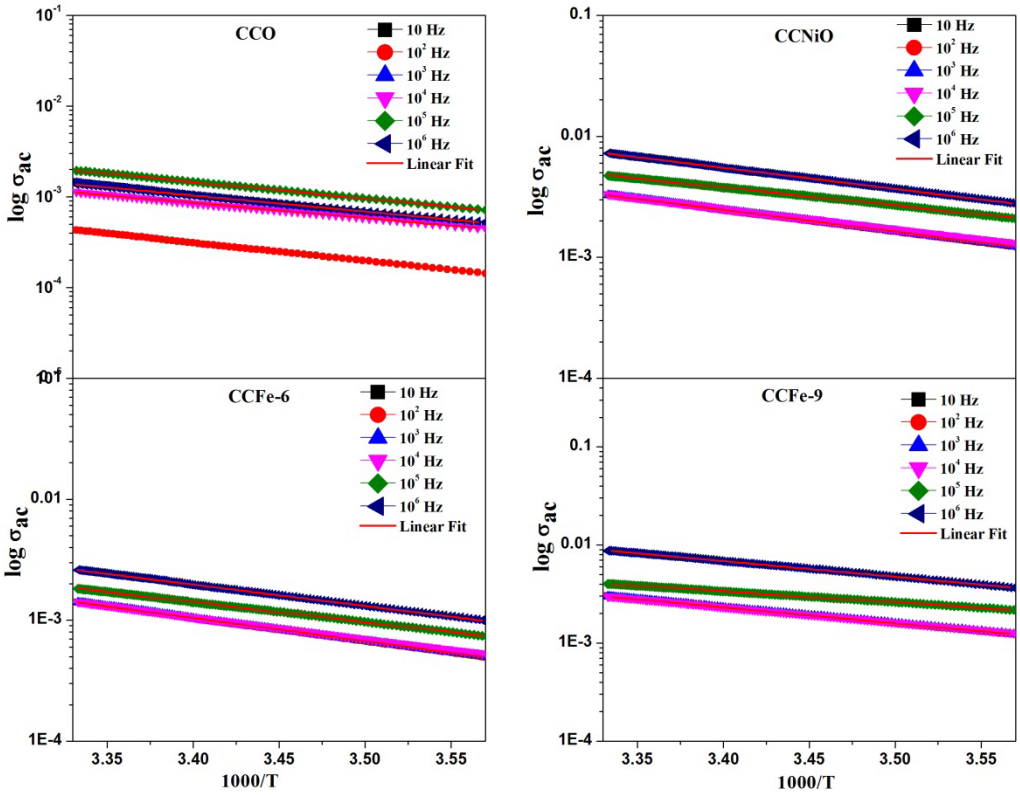

Figure 5.14: Arrhenius fit for $CuCrO_2$ and $CuCr_{0.96}Ni_{0.04}O_2$and $CuCr_{1-x}FeO_2$(x = 0.06 and 0.09) samples near room temperature.

Table 5.4: Calculated activation energies for the pure and doped $CuCrO_2$ samples

Sample	Activation energy Ea (meV)	
	10 Hz	10^6 Hz
CCO	396	362
CCTiV	413	241
CCMnV	287	186
CCGaV	382	368
CCNbV	357	338
CCVO	319	309
CCNiO	357	341
CCFe-6	361	350
CCFe-9	323	317

Figure 5.15 represents the frequency-dependent ac conductivity for some of the samples. It can be observed that the ac conductivity increases with an increase in frequency as also observed from the above Arrhenius plots. As the frequency increases, σ_{ac} also increases and the polarization decreases with increasing frequency. This also leads to an increase in eddy

current which increases the dielectric loss. Results are in agreement with the literature where it is recommended that the electrical conductivity increase with the rise in frequencyand it is due to the gradual decrease in resistance [24–26]. Thus, the change in conductivity is an outcome of thereordering and reorganization of charges at the grain boundaries of the sample under exterior temperature or electric field and interface polarization.

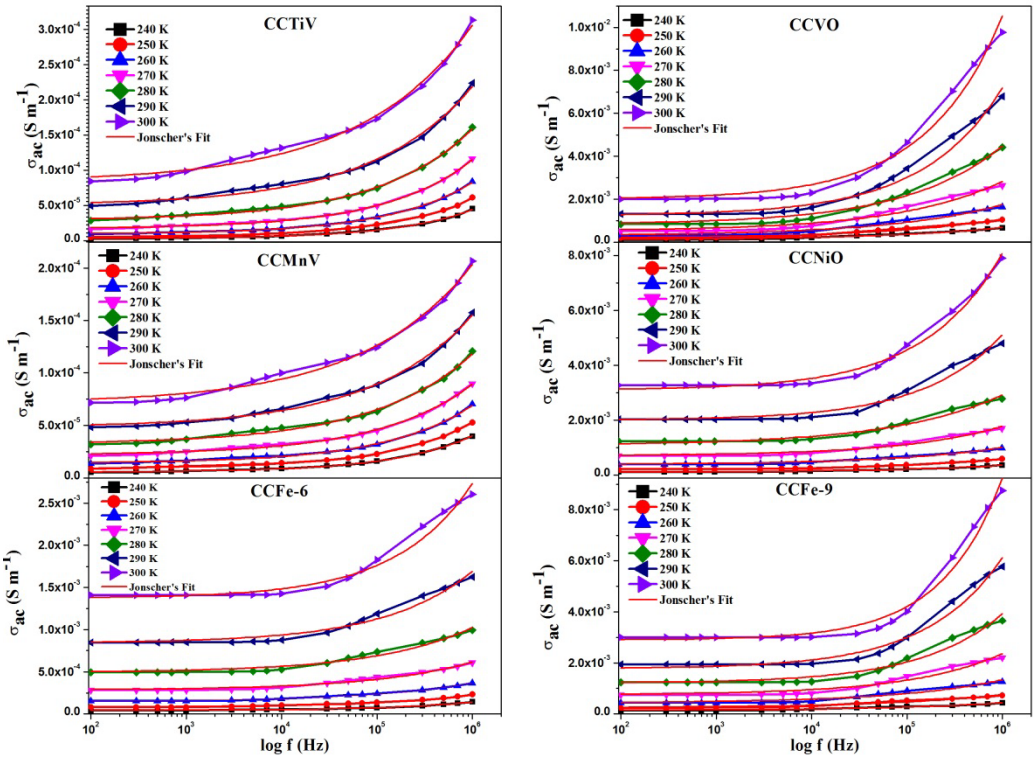

Figure 5.15: Jonscher Power Law fitof electrical conductivity for $CuCr_{0.96}M_{0.03}V_{0.01}O_2$ (M = Ti, and Mn), $CuCr_{0.96}V_{0.04}O_2$, $CuCr_{0.97}Ni_{0.03}O_2$ and $CuCr_{1-x}FeO_2$(x = 0.06 and 0.09).

Since with the increase in frequency**,** there is an enhancement of the σ_{ac}, thereby indicating that the conduction process fundamentally occurs by the small polaron hopping between localized states. In order to strengthen information regarding the conduction mechanism of the ac conductivity, Jonscher's power law can be fitted by using equation 5.4. Figure 5.15 shows the fitted curves for some of the samples. For all the samples it was found that the value of 'n' parameter varied between 0-1 (figure 5.16). Thus it can be inferred that the conduction mechanism corresponds to translational motion with a sudden hopping in the samples [13]. For all the samples except for Ti and Mn-doped the value of 'n' parameter decreases with an increase in temperature which is related to the Correlated Barrier Hopping model [27]. For other samples, the value of 'n' parameter increases with anincrease in

temperature corresponding to the non-overlapping small polaron tunneling model (NSPT) [14].

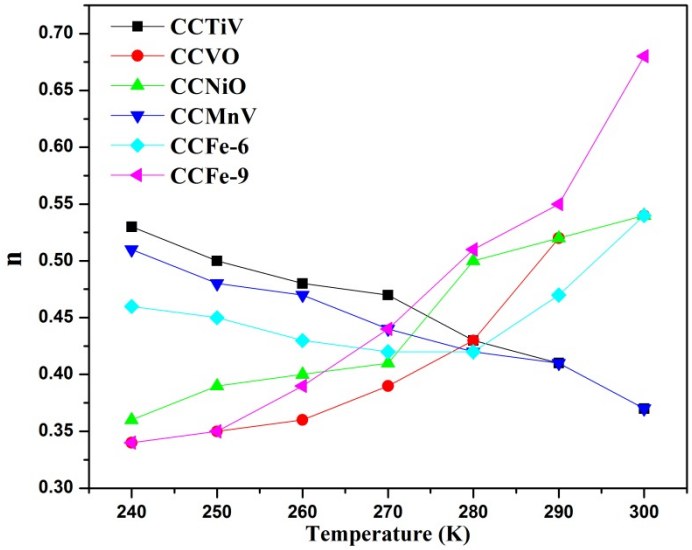

Figure 5.16: Variation of exponent 'n' of Jonscher power law vs Temperature

5.2 Conclusions

Following conclusions can be drawn from the above studies:

- For $CuFeO_2$ samples, the electric resistivity decreased with the partial substitution at the Fe site, correlated to the changes in mobility as well carrier concentration due to induced charges and MO_6 based distortions**.** Also, the electrical conductivity analysis for the CFO and CFTiV samples showed small polaron-based conductivity in these samples. Additionally, Jonscher's law based calculations through the exponent 'n' values showed an increasing trend for both the samples, confirming NSPT model-based behavior for conduction.
- For $CuCrO_2$ samples, the changes in the valence band density of states governed by the mobile holes significantly alter the low-temperature electrical conductionbehavior with the electron or hole doping in these predominantly phonon-driven semiconducting systems. The ac conductivity analysis here also confirmed **a** predominantly small polaron hopping process. However, the Jonscher's power law analysis showed that for Ti and Mn-doped samples, the conductivity is attributed to

correlated barrier hopping model, while for samples with other substitutions it is related to theNSPT model.

References

[1] P. Dordor, J.P. Chaminade, A. Wichainchai, E. Marquestaut, J.P. Doumerc, M. Pouchard, P. Hagenmuller, A. Ammar, Crystal growth and electrical properties of $CuFeO_2$ single crystals, J. Solid State Chem. 75 (1988) 105–112. https://doi.org/10.1016/0022-4596(88)90307-6.

[2] K. Shyam Prasad, A. Rao, K. Tyagi, N. Singh Chauhan, B. Gahtori, S. Bathula, A. Dhar, Enhanced thermoelectric performance of Pb doped Cu_2SnSe_3 synthesized employing spark plasma sintering, Phys. B Condens. Matter. 512 (2017) 39–44. https://doi.org/10.1016/j.physb.2017.02.021.

[3] C.J. Benedict, A. Rao, G. Sanjeev, G.S. Okram, P.D. Babu, A systematic study on the effect of electron beam irradiation on structural, electrical, thermo-electric power and magnetic property of $LaCoO_3$, J. Magn. Magn. Mater. 397 (2016) 145–151. https://doi.org/10.1016/j.jmmm.2015.08.111.

[4] N. B.s, A. Rao, P.D. Babu, G.S. Okram, Structural, electrical, magnetic and thermal properties of $Gd_{1-x}Sr_xMnO_3$ ($0.2 \leq x \leq 0.5$) manganites, Phys. B Condens. Matter. 479 (2015) 10–20. https://doi.org/10.1016/j.physb.2015.09.025.

[5] P. Mannu, M. Palanisamy, G. Bangaru, S. Ramakrishnan, A. Kandasami, P. Kumar, Temperature-dependent AC conductivity and dielectric and impedance properties of ternary In–Te–Se nanocomposite thin films, Appl. Phys. A Mater. Sci. Process. 125 (2019) 1–13. https://doi.org/10.1007/S00339-019-2751-1/FIGURES/10.

[6] A. Shukla, R.N.P. Choudhary, Study of aliovalent modification on dielectric and ac conductivity properties in lead titanate nanoceramics, J. Mater. Sci. Mater. Electron. 22 (2011) 1222–1228. https://doi.org/10.1007/S10854-011-0289-X/FIGURES/8.

[7] A. Chawla, A. Singh, M. Singh, P.S. Malhi, Small polaron hopping-assisted electrical conduction and relaxation in BCT and Mn-doped BCT samples, J. Asian Ceram. Soc. 7 (2019) 558–568. https://doi.org/10.1080/21870764.2019.1693683.

[8] R.S. Devan, B.K. Chougule, Effect of composition on coupled electric, magnetic, and dielectric properties of two phase particulate magnetoelectric composite, J. Appl. Phys. 101 (2007) 014109. https://doi.org/10.1063/1.2404773.

[9] R.P. Mahajan, K.K. Patankar, M.B. Kothale, S.A. Patil, Conductivity, dielectric

behaviour and magnetoelectric effect in copper ferrite-barium titanate composites, 2000.

[10] E.M. Benali, A. Benali, M. Bejar, E. Dhahri, M.P.F. Graca, M.A. Valente, B.F.O. Costa, Structural, morphological, Raman, dielectric and electrical properties of $La_{1-2x}Ba_xBi_xFeO_3$ ($0.00 \leq x \leq 0.20$) compounds, RSC Adv. 11 (2021) 36148–36165. https://doi.org/10.1039/D1RA05299C.

[11] S. Bhattacharyya, S.S.N. Bharadwaja, S.B. Krupanidhi, Alternating current conduction behavior of excimer laser ablated $SrBi_2Nb_2O_9$ thin films, J. Appl. Phys. 88 (2000) 4294. https://doi.org/10.1063/1.1287782.

[12] A.K. Jonscher, Dielectric relaxation in solids, J. Phys. D. Appl. Phys. 32 (1999) R57. https://doi.org/10.1088/0022-3727/32/14/201.

[13] B.N. Parida, P.R. Das, R. Padhee, S. Behera, R.N.P. Choudhary, Structural, dielectric and electrical properties of a new tungsten bronze ferroelectric ceramics, J. Mater. Sci. Mater. Electron. 25 (2014) 2618–2626. https://doi.org/10.1007/S10854-014-1920-4/FIGURES/6.

[14] J.T. Gudmundsson, H.G. Svavarsson, S. Gudjonsson, H.P. Gislason, Frequency-dependent conductivity in lithium-diffused and annealed GaAs, Phys. B Condens. Matter. 340–342 (2003) 324–328. https://doi.org/10.1016/J.PHYSB.2003.09.082.

[15] A. Maignan, C. Martin, R. Frésard, V. Eyert, E. Guilmeau, S. Hébert, M. Poienar, D. Pelloquin, On the strong impact of doping in the triangular antiferromagnet $CuCrO_2$, Solid State Commun. 149 (2009) 962–967. https://doi.org/10.1016/j.ssc.2009.02.026.

[16] T. Okuda, N. Jufuku, S. Hidaka, N. Terada, Magnetic, transport, and thermoelectric properties of the delafossite oxides $CuCr_{1-x}Mg_xO_2$ ($0 \leq x \leq 0.04$), Phys. Rev. B - Condens. Matter Mater. Phys. 72 (2005). https://doi.org/10.1103/PhysRevB.72.144403.

[17] T. Okuda, Y. Beppu, Y. Fujii, T. Onoe, N. Terada, S. Miyasaka, Specific heat of delafossite oxide $CuCr_{1-x}Mg_xO_2$ ($0 \leq x \leq 0.03$), Phys. Rev. B - Condens. Matter Mater. Phys. 77 (2008) 134423. https://doi.org/10.1103/PHYSREVB.77.134423/FIGURES/5/MEDIUM.

[18] F. Lin, C. Gao, X. Zhou, W. Shi, A. Liu, Magnetic, electrical and optical properties of

p-type Fe-doped $CuCrO_2$ semiconductor thin films, J. Alloys Compd. 581 (2013) 502–507. https://doi.org/10.1016/J.JALLCOM.2013.07.160.

[19] N. Duan, A.W. Sleight, M.K. Jayaraj, J. Tate, Transparent p-type conducting $CuScO_{2+x}$ films, Appl. Phys. Lett. 77 (2000) 1325. https://doi.org/10.1063/1.1289906.

[20] A.N. Banerjee, C.K. Ghosh, K.K. Chattopadhyay, Effect of excess oxygen on the electrical properties of transparent p-type conducting $CuAlO_{2+x}$ thin films, Sol. Energy Mater. Sol. Cells. 89 (2005) 75–83. https://doi.org/10.1016/J.SOLMAT.2005.01.003.

[21] D. Li, X. Fang, A. Zhao, Z. Deng, W. Dong, R. Tao, Physical properties of $CuCrO_2$ films prepared by pulsed laser deposition, Vacuum. 84 (2010) 851–856. https://doi.org/10.1016/J.VACUUM.2009.11.014.

[22] N. Barot, P.K. Mehta, A. Rao, R. Thomas, Y.-K. Kuo, Effects of iso- and polyvalent substitutions on the short/long-range crystalline order in $CuCrO_2$ compounds, J. Alloys Compd. 791 (2019). https://doi.org/10.1016/j.jallcom.2019.03.291.

[23] L. Shi, G. Li, S.J. Feng, X.G. Li, Effect of Sb doping on the structure and transport properties of the Ru-1222 system, Phys. Status Solidi. 198 (2003) 137–141. https://doi.org/10.1002/PSSA.200306455.

[24] I.M. Afandiyeva, M.M. Bülbül, S. Altindal, S. Bengi, Frequency dependent dielectric properties and electrical conductivity of platinum silicide/Si contact structures with diffusion barrier, Microelectron. Eng. 93 (2012) 50–55. https://doi.org/10.1016/J.MEE.2011.05.041.

[25] A.A. Sattar, S.A. Rahman, Dielectric Properties of Rare Earth Substituted Cu–Zn Ferrites, Phys. Status Solidi. 200 (2003) 415–422. https://doi.org/10.1002/PSSA.200306663.

[26] P. Dutta, S. Biswas, S. De Kumar, Dielectric relaxation in polyaniline–polyvinyl alcohol composites, Mater. Res. Bull. 37 (2002) 193–200. https://doi.org/10.1016/S0025-5408(01)00813-3.

[27] G.E. Pike, ac Conductivity of Scandium Oxide and a New Hopping Model for Conductivity, Phys. Rev. B. 6 (1972) 1572. https://doi.org/10.1103/PhysRevB.6.1572.